ADVANCED MATERIALS INTERFACES
www.advmatinterfaces.de

Optofluidic Platform for the Manipulation of Water Droplets on Engineered $LiNbO_3$ Surfaces

*Annamaria Zaltron, Davide Ferraro, Alessio Meggiolaro, Sebastian Cremaschini, Mattia Carneri, Enrico Chiarello, Paolo Sartori, Matteo Pierno, Cinzia Sada, and Giampaolo Mistura**

The actuation and control of liquid droplets on a surface have important implications in many industrial applications and microfluidics. In recent years, various strategies have been used. Here, an optofluidic platform that performs the basic droplet handling operations required in a common microfluidic device is presented. It is based on z-cut, iron-doped lithium niobate crystals that, when illuminated, generate surface charges of opposite sign at the two crystal faces because of the photovoltaic effect. The face of the crystal in contact with the droplets is coated with a lubricant-infused layer, which guarantees hydrophobicity and, more importantly, a very slippery and robust surface for prolonged use. In this way, sessile water droplets having volumes of microliters, corresponding to millimeters in size, can be easily actuated, guided, merged, and split by projection on the crystal of suitable static or dynamic light patterns. The actuated droplets can cover distances of centimeters on a timescale of a few seconds. The resulting platform is highly flexible and reconfigurable and does not require moving parts.

1. Introduction

Controlled transport of liquid droplets on solid surfaces is a key function for several industrial processes,[1] such as heat transfer, water harvesting, energy generation, printing, and even clinical diagnostics, to name a few. Droplet control can be achieved using passive or active approaches.[1] Passive control can be obtained by printing a hydrophilic path on an otherwise hydrophobic surface.[2] More generally, the presence of domains of different wettability introduces interfacial forces that affect the droplet dynamics.[3] For instance, parallel stripes can slow down, deviate,[4] or induce nonlinearities[5] in the drop motion. If the pattern is not symmetric, such as an array of triangular domains,[6] the motion can be anisotropic. Novel biomimetic functional surfaces, known as liquid-infused surfaces (LISs),[7] allow easy manipulation of small drops; for example, droplets with volume ≤2 µL deposited on a LIS begin to move at inclination angles even below 5°. These surfaces are textured materials that are usually imbibed with fluorinated oils. The premise for such a design is that the liquid surface is intrinsically smooth and defect-free down to the molecular scale, provides immediate self-repair by wicking into damaged sites in the underlying substrate, is largely incompressible, and can be chosen to repel immiscible liquids of virtually any surface tension and viscosity.[7b,8]

Active control on functionalized surfaces can instead be realized with an ample variety of external stimuli,[1c] which include electric[9] and magnetic[10] fields, light,[11] temperature gradients,[12] and acoustic vibrations.[13] In particular, electrowetting on dielectrics is one of the most efficient and robust methods to manipulate drops, thanks to its fast response time and the large forces achievable from millimeter to micrometer scale.[14] However, it requires the realization of electrodes and their cumbersome connection to voltage suppliers. This limitation also holds in the case of opto-electrowetting, where the voltage bias of photoconductors is needed to induce light-assisted phenomena.[15]

A promising viable alternative to the presence of electrodes deposited on a substrate is based on the photovoltaic effect exhibited inside certain ferroelectrics, such as iron-doped lithium niobate, Fe:$LiNbO_3$, which consists of a nonsymmetrical light-induced excitation of electrons from donor centers that causes charge transport mainly along the polar axis (*c*-axis) of the crystal.[16] Upon appropriate illumination, an electric field is generated within the material with a strength that can even be as high as 100–200 kV cm^{-1} and the photoinduced charges are redistributed on the surface.[17] This photoinduced electric field extends outside the active optical material (evanescent field) and is able to manipulate micro- and nano-objects, mainly through dielectrophoretic forces.[18] More recently, the photovoltaic effect has also been exploited to manipulate water droplets. Fan et al. succeeded in photovoltaic manipulation of nanoliter droplets on Fe:$LiNbO_3$ coated with a hydrophobic Teflon film.[19] However, this study involves only very tiny

A. Zaltron, D. Ferraro, A. Meggiolaro, S. Cremaschini, M. Carneri, E. Chiarello, P. Sartori, M. Pierno, C. Sada, G. Mistura
Dipartimento di Fisica e Astronomia "G. Galilei"
Università di Padova
via Marzolo 8, Padova 35131, Italy
E-mail: giampaolo.mistura@unipd.it

The ORCID identification number(s) for the author(s) of this article can be found under https://doi.org/10.1002/admi.202200345.

DOI: 10.1002/admi.202200345

droplets (volume $\Omega \approx 0.3$ nL) moving at low speed (≈10 µm s^{-1}) over distances of a few hundreds of micrometers, which are not very useful for microfluidic applications due to their rapid evaporation and small displacements. To reduce friction forces on the solid surface, Puerto et al. investigated aqueous droplets that hang by a density gradient at the fluid interface between a thick (≈2 mm) oil layer and air;[20] in spite of such an unusual configuration for open microfluidics, the fields generated by the bulk photovoltaic effect in the $LiNbO_3$ substrate allowed droplet manipulation and splitting. Finally, Tang et al. reported the self-propulsion of water droplets on $LiNbO_3$ crystalline surfaces due to the generation of surface electric potential through thermoelastic–piezoelectric coupling.[21]

In this work, we present a hybrid substrate formed by an iron-doped lithium niobate crystal coated with a slippery LIS (Fe:$LiNbO_3$/LIS) that provides a robust platform for passive and active control of water droplets. The very low friction of these lubricated surfaces allows for the actuation of droplets without the use of very intense light sources. The near absence of chemical defects and surface asperities guarantees a much higher reproducibility than that of standard solid surfaces. They are also found to be fully compatible with the presence of laser beams and are highly resistant to the prolonged passage of droplets. After analyzing the interaction between an illuminated area and a liquid drop, we demonstrate fast actuation (approximately seconds) of large sessile water droplets (approximately microliters) over macroscopic distances (approximately centimeters), all figures encountered in standard applications in open surface microfluidics.[22] Control is achieved by activating virtual electrodes obtained by projecting suitable optical patterns onto the crystal using a laser beam impinging on a spatial light modulator. Accordingly, the experimental setup does not involve any moving parts. In addition, the platform is easily reconfigurable, flexible, and guarantees high reproducibility.

2. Experimental Section

2.1. Iron-Doped Lithium Niobate Crystals

Commercial *z*-cut iron-doped lithium niobate crystals supplied by PI-KEM Limited (single domain crystals with diameter of 3 in. and thickness of 1 mm) were used. For this crystal cut, the polar axis *c* was perpendicular to the circular main faces oriented parallel to the *z*-axis, see **Figure 1**. In this configuration, the bulk photovoltaic current arising inside the material under illumination led to an accumulation of surface charges of opposite sign at the two crystal faces. Doping the material with iron ions could significantly enhance this phenomenon. The samples had a uniform iron concentration of 0.1% mol (18.8×10^{18} at cm^{-3}), which guaranteed an optimal photovoltaic response of the materials.[23] The amount of donor ions Fe^{2+} was derived by optical absorption measurements (with a Jasco V-670 spectrophotometer) in the range of 300–2000 nm[24] and was equal to $(4.6 \pm 0.1) \times 10^{18}$ at cm^{-3}, leading to a degree of reduction $R = [Fe^{2+}]/[Fe^{3+}] = 0.32 \pm 0.01$.

2.2. Preparation of LISs

The Fe:$LiNbO_3$ crystal was coated with a LIS. In detail, an ≈25 µm thick porous polytetrafluoroethylene (PTFE) membrane (Sterlitech Corporation) was placed on the +*z* face of the crystal. Once the membrane was gently placed on the Fe:$LiNbO_3$ surface, ethanol was pipetted onto the entire sample and left to evaporate, leading to spontaneous mechanical adhesion of the membrane to the crystal.[13b] With a dip coater (Kibron Inc. LayerX 274), the membrane attached to the Fe:$LiNbO_3$ surface was infused with fluorinated oil (Fomblin perfluoropolyether Y LVAC 06/6) with viscosity of 120 mPa s at $T = 20$ °C, using the procedure reported in.[25] The withdrawal velocity during dip

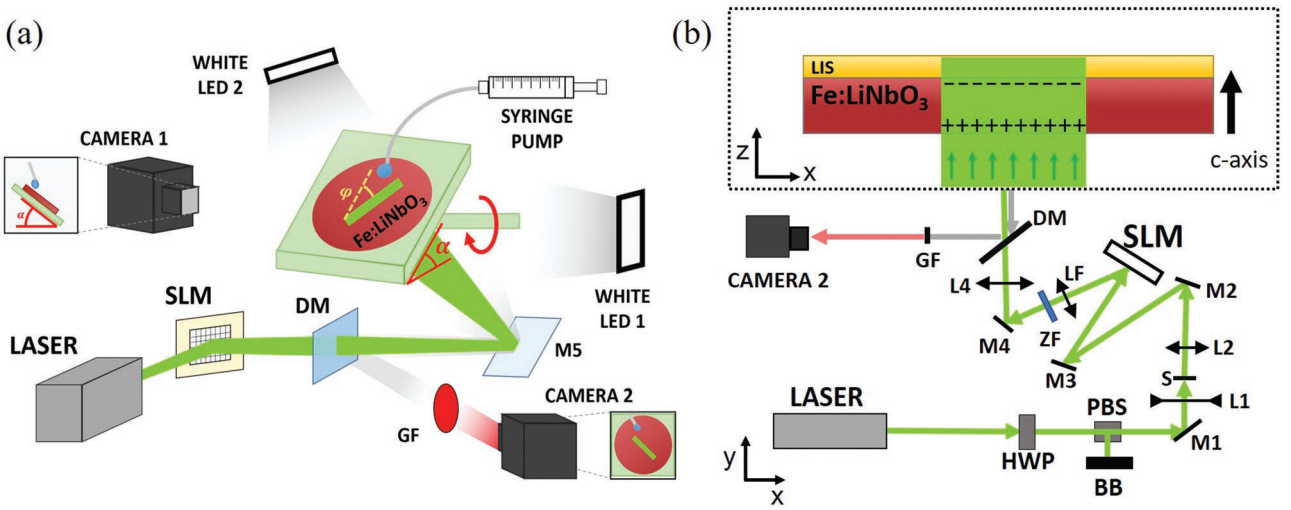

Figure 1. a) Droplets generated with a syringe pump are gently deposited on the tilted Fe:$LiNbO_3$/LIS sample through a PTFE capillary. Camera 1, in front of LED 1, records the droplet from the side, while camera 2 records the droplet from the bottom of the sample, illuminated by LED 2 whose light is reflected from the mirrors M5 and, partially, from the dichroic mirror (DM). A red-pass filter GF is placed before camera 2 to stop the laser straylight. b) Scheme of the optical path followed by the laser beam to project a light pattern on the Fe:$LiNbO_3$ crystal coated with a lubricant-infused surface (LIS). See the main text for further details.

coating was set at 0.12 mm min^{-1}, according to the Landau–Levich equation,[26] to ensure a controlled thickness of the liquid layer above the membrane of ≈0.5 µm. Thicker layers led to less reproducible results in terms of droplet guiding; differently, thinner layers required longer times for the impregnation process (>24 h).

2.3. Optofluidic Setup

The experimental setup used in this work is shown schematically in Figure 1a. Ultrapure water droplets (resistivity 18.2 MΩ cm) of known volume were generated with a computer-controlled syringe pump (PHD 22/2000, Harvard apparatus) equipped with a glass syringe (1 mL, SGE) connected to a PTFE capillary (0.3/0.6 mm internal/external diameter, Merck), which could be fixed near the sample. In this way, single or trains of droplets could be produced with a volume between 1 and 20 µL, with an accuracy of ≈2%. The time interval separating two consecutive droplets could be varied between 2 s and tens of seconds, with an accuracy of about 0.1 s. The hybrid substrate was mounted on a motorized 3-axis stage (M-126CG, PI) equipped with a customized rotation mount, which allowed the angle of inclination to be varied with respect to the horizontal plane.

Moving droplets could be viewed from the side and bottom using two independent charged coupled device cameras (Basler acA1300-200 µm), equipped with optical zoom lenses (respectively, Baumer Linos and Navitar MVL 7000). White light emitting diode (LED) lights were used to illuminate the sample. Camera 1 was used to view the lateral profile of the droplet, camera 2 was placed below the sample and aligned to record the droplet through the sample. In detail, light 2 illuminated the droplet from the top and was first reflected by a mirror (M5) fixed below the sample holder and then by a dichroic mirror (MD568, Thorlabs) used for optical pattern generation. The dichroic mirror was chosen to pass the green light (532 nm) from the laser and reflected the red component of the white LED light used to back-illuminate the sample. An emission filter (MF620-52, Thorlabs), GF in Figure 1a, was placed before the camera to remove any residual back reflection of the laser beam. The acquired images were analyzed with ImageJ.

The Fe:$LiNbO_3$ crystal could be illuminated with an optical pattern produced with the setup shown in Figure 1b. The laser source (Azur Light Systems, max output power 1 W, $\lambda = 532$ nm) was kept at constant output power for optimal stability. The linearly polarized laser beam was attenuated by a combination of a half-wave plate (HWP) mounted on a computer-controlled goniometer and a polarizing beam splitter (PBS) and a beam block (BB). The diameter of light beam was increased from 1.5 to 8 mm by a beam expander (lenses L1 and L2) and collimated toward the spatial light modulator (SLM, Pluto-NIR-011, Holoeye Photonics), coupled with a Fourier lens (LF). The SLM was capable to axially separate the desired light pattern from the residual undiffracted zeroth-order, which was blocked with a filter (ZF) at the Fourier plane. A lens (L4) magnified and focused the resulting image on the Fe:$LiNbO_3$ sample. Finally, a properly tilted mirror (M5), see Figure 1a, ensured that incident light illuminated the crystal perpendicularly to its main surfaces from the bottom. Taking into account the losses of the optical components, the power P of the light pattern impinging on the sample could vary between 0 and 135 mW, and a computer-controlled mechanical shutter (S) allowed control of the exposure time.

2.4. Statistical Analysis

The data presented in the graphs of the paper are the average results of at least three independent measurements and the standard deviations are taken as representative errors.

3. Results and Discussions

To better assess the capabilities of this hybrid substrate in controlling the motion of a droplet over a surface, we separately discuss the passive control obtained by designing the path followed by droplets driven by gravity and the active control where droplets are actuated on a horizontal surface by the action of the laser beam. This distinction is further justified by the difference in illumination intensity I, since the droplet actuation requires an intensity that is two orders of magnitude higher than that employed for the passive guidance. Before describing the droplet control results, we present in some detail the performance of the lubricated coating, which is an essential component of our platform.

3.1. Lubricated Coating Stability

For this application, the lubricated infused surface consists of a porous filter placed on one face of the $LiNbO_3$ crystal and infused with fluorinated oil. We have chosen this approach[14b] because it does not require complicated protocols, including heating processes that could damage the pyroelectric $LiNbO_3$ crystal. To ensure high reproducibility, a dip-coater is used for the oil impregnation. In this way, it is possible to produce oil films with a controlled thickness of ≈0.5 µm. We found that this thickness allows for good slippage and robust performance, see Section S1 of the Supporting Information for more details. The LIS performance was tested by analyzing the speed of repeated sequences of water droplets with different volumes (Ω = 5–15 µL) and descending at different tilt angles (between 15° and 45°). We found that LIS could be used safely for the motion of thousands of droplets, corresponding to about a week of laboratory use, see Section S2 of the Supporting Information for more details. When the droplets started to pin on the surface, the LIS was regenerated by repeating the dip-coating process. Keeping the lubricated sample in a sealed Petri dish for one month to prevent dust did not cause any appreciable variation in the sliding performance. Its stability was also tested by exposing the LIS to high intensities, of the same order as those used for droplet actuation ($I \approx 20$ kW m^{-2}), but for much longer times (about 15 min); no variation was detectable in either the surface contour or reproducibility of the experiments presented in the following paragraphs. Since the presence of residual charges on the

substrate can affect the motion of the droplets, before each experimental run, we verified that the $LiNbO_3$ crystal was discharged using the pendant droplet method.[27] The complete discharge of the $LiNbO_3$ crystal was obtained after its immersion in a water tank for 20 min. We checked that such a procedure did not affect the LIS wetting behavior, see Section S2 of the Supporting Information for more details.

3.2. Passive Control

Arguably, one of the simplest realizations of passive control is the deviation of the trajectory of a train of droplets moved by gravity. **Figure 2** summarizes the results obtained by depositing water droplets on a Fe:$LiNbO_3$/LIS optically imprinted with a stripe pattern. The sample is tilted at an angle $\alpha = 30°$ with respect to the horizontal direction, while the stripe is inclined at an angle $\varphi = 45°$ with respect to the vertical downward direction. The linear stripe, with dimensions 32×2 mm^2, is obtained by illuminating the crystal with the pattern produced by a SLM with $I \approx 600$ W m^{-2}, corresponding to a light power P of 40 mW, for a time interval of 2 min. After that, the laser is turned off and droplets with a volume of 4 µL are gently deposited on the surface. Snapshots (a)–(d) show the position of the first droplet as viewed from the bottom of the sample at subsequent times. The dashed lines highlight the trajectory followed by the droplet, whereas the green rectangle indicates the area previously illuminated by the laser. Initially, the droplet moves downward (a) until it reaches the edge of the illuminated stripe (b). Then, the droplet follows the top edge of the stripe (c) mainly due to the dielectrophoretic attraction to photoinduced charges.[20] The dielectrophoretic force arises from the electric interaction between the photovoltaic field E_{pv} outside the crystal (evanescent field) and the induced dielectric polarization of the droplet. The interaction between a nonuniform evanescent field and a neutral, dielectric body can be approximated as[18e–i,28]

$$\boldsymbol{f} = -\nabla\left(\boldsymbol{p}\cdot\boldsymbol{E}_{pv}\right) \sim -\nabla \boldsymbol{E}_{pv}^2 \tag{1}$$

where p is the induced polarization. In the case of a homogeneous spherical particle of radius r and relative dielectric permittivity ε_p, immersed in a fluid of relative dielectric permittivity ε_f, the magnitude of this force is given by the simple equation[18b,d,h]

$$f = 2\pi\varepsilon_f r^3 \Re\left(K(\omega)\right)\nabla E_{pv}^2 \tag{2}$$

where $\Re(K(\omega))$ is the real part of the Clausius–Mossotti factor $K(\omega) = (\varepsilon_p^* - \varepsilon_f^*)/(\varepsilon_p^* + 2\varepsilon_f^*)$ and ε^* is the complex dielectric permittivity. If we assume a spherical droplet of ultrapure water ($\varepsilon_p = 80$, electrical conductivity $\sigma = 5.5$ µS m^{-1}) immersed in air ($\varepsilon_f = 1, \sigma \lesssim 10^{-4}$ µS m^{-1}), the droplet will be always attracted toward regions of high field strength. Recently, Munoz-Martinez et al. considered a detailed model based on the complete system of rate equations and used the finite element method to calculate the electric field and the space charge distribution in z-cut Fe:$LiNbO_3$ crystals under different illumination patterns.[18i] In the case of a circular and uniformly illuminated spot, the dielectrophoretic force is oriented toward the edge of the illumination where it is highest. This explains why, in the snapshots of Figures 2–4, the droplets are observed

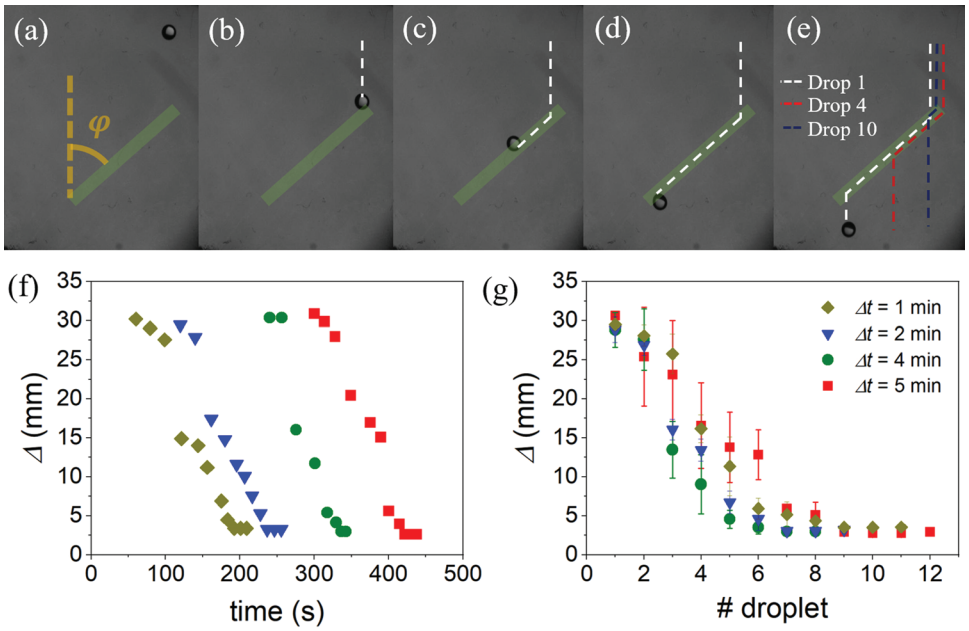

Figure 2. a–d) Sequence of consecutive video frames taken from the bottom of the Fe:$LiNbO_3$/LIS sample, showing the movement of a 4 µL drop along a previously illuminated stripe inclined at $\varphi = 45°$ with respect to the vertical direction, schematically indicated in the images. The Fe:$LiNbO_3$/LIS sample, tilted at $\alpha = 30°$ to the horizontal, was illuminated for 2 min at $I = 625$ W m^{-2} and the video was taken immediately after the laser turn off. e) Trajectories followed by the first, fourth, and tenth droplets of the same train of droplets. f) Distance traveled by consecutive droplets along the stripe (Δ) as a function of the time from laser turnoff and g) of the number of passing droplets for different delay times Δt.

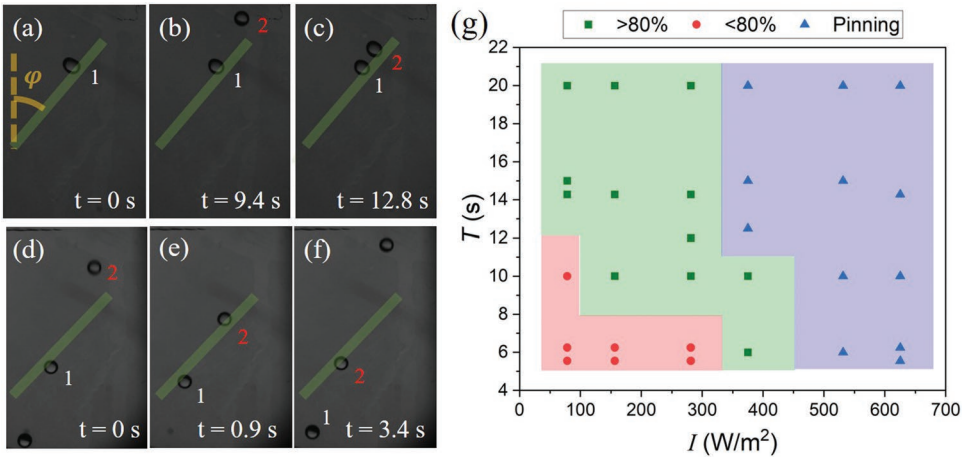

Figure 3. a–c) Sequence of consecutive video frames taken from the bottom, showing the movement of 5 µL droplets that are pinned to the illuminated area, for $T = 10$ s and $I \approx 530$ W m^{-2}. d–f) Sequence of consecutive video frames showing droplets continuously deviated by the illuminated stripe, for $T = 6$ s and $I \approx 375$ W m^{-2}. Numbers are added to track the same droplet along the frames. In both cases, the Fe:$LiNbO_3$/LIS sample is tilted by $\alpha = 30°$ and the stripe is inclined by $\varphi = 45°$. g) Phase diagram summarizing all acquired data, varying T and I, reporting when more than 80% of the droplets follow the illuminated stripe (green), less than 80% of the droplets follow the illuminated stripe (red), and when the droplets are pinned to the substrate (blue).

to move along the edge of the stripes. When the drop reaches the end of the stripe in Figure 2d, it recovers its vertical motion because the attraction to the stripe decreases and the droplet dynamics is only regulated by the gravity force. The next droplet is found to follow the same trajectory. However, the subsequent ones follow the stripe progressively less: Figure 2e displays with different colors the trajectories of the first, fourth, and tenth droplets. It is clear that the guide effect disappears after ≈10 droplets, suggesting a progressive discharge of the virtual electrode.

To better investigate this effect, we illuminated the crystal for 2 min and varied the time interval between laser turnoff and deposition of the first droplet between 1 and 5 min (delay time, Δt). Trains of droplets of volume $\Omega = 4$ µL were generated with a syringe pump and deposited at a distance of about 5 mm above the stripe. The time interval T between two consecutive droplets was set at $T = 15$ s. For each consecutive droplet, the distance Δ traveled along the stripe was measured and, in Figure 2f, is plotted against the arrival time when the droplet first reaches the previously illuminated stripe corresponding to the snapshot (b). To guarantee reproducible conditions, the illumination of the stripe always starts from the crystal fully discharged. The resulting curves look quite similar and only shifted by the delay time Δt, suggesting that the discharge of the virtual electrode is due to the moving droplets and not to the intrinsic processes occurring in the crystal lattice. This fact is also confirmed by the behavior of the photovoltaic effect in Fe:$LiNbO_3$, which shows a decay of light-induced charge accumulations, once the illumination has been turned off, occurring on a timescale of hours or days.[29] The graph in Figure 2g, where the same data are plotted as a function of the droplet number, indicates that the passive control disappears, that is, $\Delta \approx 0$, after ≈6 or 7 drops, regardless of the delay time Δt.

The observed discharge of the stripe is probably due to the detachment of small charged fragments from the water droplets induced by the photovoltaic field.[30] We tried to directly observe these fragments, but no conclusive proof was found, see Section S3 of the Supporting Information for more details. Indirect evidence of these fragments was obtained by illuminating with a laser a water droplet deposited on a Fe:$LiNbO_3$/LIS in proximity of a metallic wire. A cycling to-and-fro motion of the water microdroplet from the laser spot to the metal surface was observed, with the droplet volume decreasing during the motion.[30b] The photovoltaic field pointing from the laser spot to the wire moves the positive and negative ions, which are present even in ideally purified water due to natural ionization.[18h] It was claimed that this interaction may lead to the breakup of the droplet in a tiny charged fragment immobilized at the laser spot, while the oppositely charged droplet moves toward the wire.[30b] The charged fragment then screens the local photovoltaic charges. Our experimental results suggest that the charged fragments start to detach from the end of the stripe and progressively discharge the whole stripe.

We can then expect that if the stripe is kept illuminated, the discharge from the droplets can be compensated for by the accumulation of new charges at the surface of the Fe:$LiNbO_3$ crystal. Therefore, the deviation induced by the illuminated stripe is the result of the interplay between the light intensity, the volume, and the generation rate of the droplet trains. In detail, if I is too high and/or the time interval T between consecutive droplets is too long, the attraction to the illuminated stripe is so high that the droplets are pinned to it, as shown in the video frames of **Figure 3**a–c, where $I \approx 530$ W m^{-2} and $T = 10$ s. Then, it is possible to find intermediate values where the illuminated stripe consistently deviates consecutive droplets, as shown in Figure 3d–f: the frames display consecutive droplets at different times following the illuminated pattern, for $I = 375$ W m^{-2} and $T = 6$ s (see also Movie S1 of the Supporting Information). To quantify the passive control exerted by the illuminated stripe, we considered the fraction ε of droplets that completely follow the stripe, for trains of at

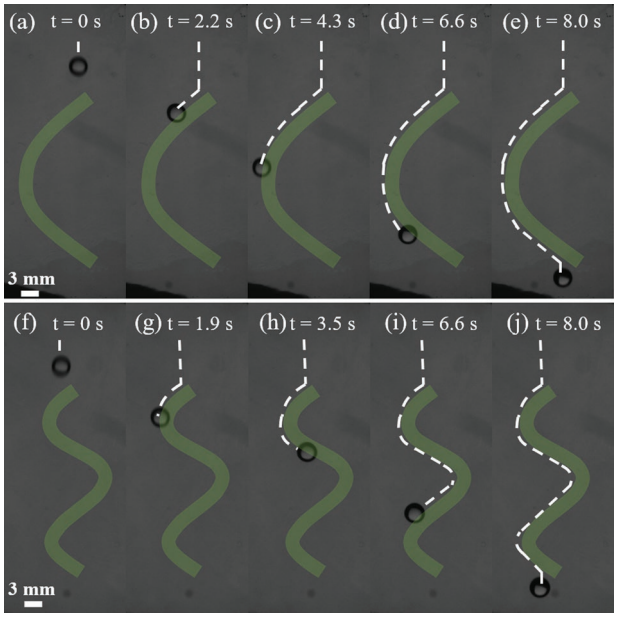

Figure 4. Sequential video frames taken from the bottom view showing the motion of a drop along illuminated a–e) semicircular and f–j) wavy stripes. The green contours represent the patterns illuminated by the laser light. The dashed lines indicate the trajectories followed by the droplets. The Fe:$LiNbO_3$/LIS sample is inclined by $\alpha = 30°$, $I \approx 100$ W m^{-2}, $T = 12$ s, and $\Omega = 5$ µL.

least 50 droplets. The results are summarized in the phase diagram shown in Figure 3g, where the green dots correspond to a fraction ε bigger than a chosen threshold of 80%, the red dots to $\varepsilon < 80\%$, and the blue dots refer to droplets that are pinned to the illuminated area. As expected, when the illumination is low ($I \approx 78$ W m^{-2}), good guidance is achieved when the droplets are generated at sufficiently long T ($T > 14$ s) to allow the stripe to charge, while increasing I (e.g., $I \approx 280$ W m^{-2}), the required T decreases ($T = 10$ s). Differently, when $I > 375$ W m^{-2} and $T > 12$ s, droplets are pinned to the illuminated area. In particular, under optimal guiding conditions ($I = 156$ W m^{-2} and $T = 13$ s), $\varepsilon > 95\%$ can be achieved, as shown in Movie S2 (Supporting Information), where more than 200 droplets are continuously guided by the illuminated stripe.

Needless to say, the passive guide exerted by the illuminated linear stripe can be extended to more complicated patterns. **Figure 4** and Movies S3 and S4 (Supporting Information) show the control achieved, respectively, with semicircular (top) and wavy (bottom) stripes optically imprinted on the Fe:$LiNbO_3$ crystal by using the spatial light modulator. Again, the droplets move preferentially along one edge of the stripes due to the dielectrophoretic attraction.[20] These examples show that it is possible to optically achieve passive control of droplets on a lubricated surface similar to that obtained on a patterned two-phase lubricant-infused surface.[31] The added advantage of the optical method is that it is easily reconfigurable.

3.3. Active Control

More important for potential applications is the active control of the droplet motion. If the illumination intensity is significantly increased, the dielectrophoretic interaction between neutral water droplets and the photoinduced charges generated at the surface of the Fe:$LiNbO_3$ crystal becomes large enough that it can actuate and guide sessile droplets. **Figure 5** and Movie S5 (Supporting Information) show the basic case of a water droplet initially at rest on a horizontal Fe:$LiNbO_3$/LIS: when a circular and uniform spot of light with a diameter $D = 3$ mm and $I \approx 11$ kW m^{-2} is produced close to its contour, see Figure 5a, charges begin to be generated at the substrate surface and the droplet is found to move toward the illuminated area within a couple of seconds, see Figure 5b–d, as also found for much smaller drops ($\Omega \approx 0.3$ nL) and much higher light intensity ($I \approx 2000$ kW m^{-2}).[19]

To take advantage of this interaction and to be able to drive droplets along designed pathways, it is essential to investigate how the response time δt of the moving droplet depends on the main physical quantities involved. In detail, after a droplet of ultrapure water of known volume Ω is gently deposited on the hybrid substrate with a micropipette, a circular spot of diameter D is illuminated at a distance d from the droplet, see **Figure 6**a. The response time δt is then determined as the time interval between the moment the light is turned on and the moment the droplet starts to move. Keeping constant the size of the spot ($D = 3$ mm) and the distance between the spot and the drop ($d = 0$ mm), Figure 6b shows that, regardless of the volume of the drop, the response time rapidly decreases with increasing I: at $I < 4.7$ kW m^{-2}, δt is of the order of tens of seconds, while for $I > 8.8$ kW m^{-2}, δt is of the order of a couple of seconds or less without a clear dependence on Ω. This fact suggests that the pulling action due to the dielectrophoretic force depends nontrivially on Ω and a precise determination of the spatial distribution of the photovoltaic field is required to explain the experimental response times, see Section S4 of the Supporting Information for more details. Instead, Figure 6c shows that, for a given I, δt rapidly increases with the size of the spot D (data refer to $\Omega = 3$ µL and $d = 0$ mm). Finally, Figure 6d shows that δt increases with d (data refer to $I = 19.1$ kW m^{-2} and $D = 3$ mm). Interestingly, in the interval between $d = -1.5$ mm, corresponding to the illuminated circle that partially overlaps the water drop, and $d = +1$ mm, the response is practically independent of volume

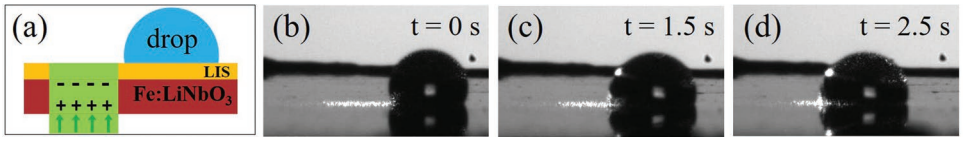

Figure 5. a) Side view of the active actuation of a droplet on Fe:$LiNbO_3$/LIS. The green arrows indicate the direction of illumination of the crystal with an intensity $I \approx 11$ kW m^{-2}. b–d) Sequential video frames of a droplet moving from right to left when the circular spot is projected on the sample surface at $t = 0$ s. In the reported example, $P = 77$ mW, $D = 3$ mm, and $\Omega = 3$ µL.

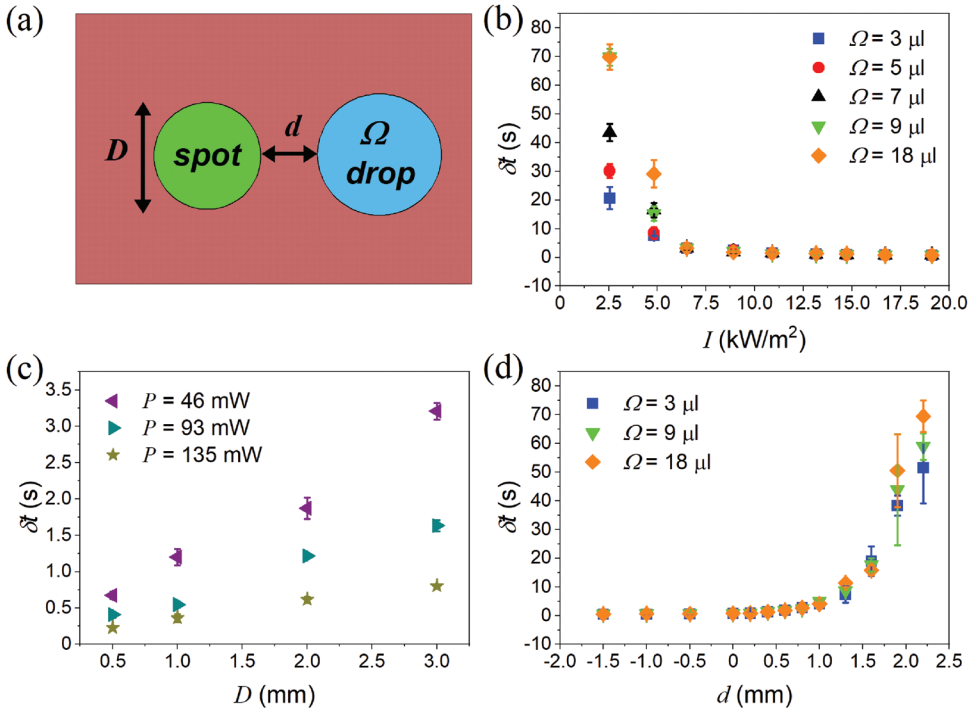

Figure 6. a) Cartoon representing the geometry of the experimental configurations. The three graphs explore the dependence of the response time δt on the main physical quantities involved: b) the intensity I of the light pattern impinging on the sample for different droplet volumes Ω and $D = 3$ mm, $d = 0$ mm; c) the diameter D of the circular spot for different I and $\Omega = 3$ µL, $d = 0$ mm; d) the distance d between the spot and the droplet for different Ω and $I \approx 19.1$ kW m^{-2}.

Ω and, more importantly, very small, on the order of 0.5 s. The final points indicate the maximum distance at which the droplet is attracted toward the illuminated area, i.e., for d longer than about 2.2 mm, the droplet does not move.

The data reported in Figure 6 can be rationalized by assuming the time evolution of the photoinduced surface charges. For a uniformly illuminated area, the surface charge density accumulated on the crystal surface after an exposure time t_{exp} can be approximated by an exponential decay function: $\sigma = \sigma_{sat}(1 - e^{-t_{exp}/\tau})$, where σ_{sat} depends on the properties of the Fe:LiNbO$_3$ crystal, while the decay time constant τ is inversely proportional to the intensity of the incident beam I.[18g,32] An important parameter can then be defined, the light exposure, defined by the product $(I \cdot t_{exp})$, which is a good indicator of the speed of the process, crucial to compare experiments performed with different intensities I.[35] The droplet starts to move when the attraction to the photoinduced charges overcomes the static friction force. Consequently, increasing I reduces the time it takes to reach the required charge density, as shown in Figure 6b. Similarly, Figure 6c shows that δt increases with the spot diameter D because, keeping P constant, the intensity I decreases with the illuminated area and then it takes longer to reach the critical charge density. Then, the fact that larger drops require a longer δt, see Figure 6a, implies that they experience a higher static friction force. This force, of capillary origin, is due to the nonuniformity of the contact angle along the perimeter of the drops, caused by the contact angle hysteresis, and scales as the length of the contact line.[33] Its effect becomes negligible for sufficiently high power ($I > 6.6$ kW m^{-2}). Finally, the graph in Figure 6d shows that the droplet motion is also induced when there is no direct contact between the light spot and the droplet contact area ($d > 0$), confirming that the actuation is due to the dielectrophoretic force.[18i,20,27]

The practical conclusion drawn from this case study is that the motion of a water droplet deposited on the hybrid substrate can be easily driven by illuminating the crystal in proximity to the droplet. Next, we show how this basic process can be exploited to achieve some of the complicated droplet handling required for microfluidic applications. We start with the optical guidance of a water droplet along a well-defined path. **Figure 7**a–f shows a sequence of video frames in which a 3 µL droplet is moved on the horizontal sample by illuminating the substrate with a uniform light spot ($I \approx 10.9$ kW m^{-2} and $D = 3$ mm), which progressively moves along a linear path, from right to left (see also Movie S6 of the Supporting Information). Similar results are also observed for a curved pattern projected on the same sample surface, as shown in Figure 7g–k: the droplet is viewed from the bottom of the sample and the circular spots that are progressively shifted are reported as green circles in the figures (see also Movie S7 of the Supporting Information). In general, the displacements of droplets of volume approximately microliter over centimeter distances can be easily obtained in <1 min.

An even simpler actuation method consists of illuminating a stripe of a given shape with a linearly varying intensity, as shown in the example of **Figure 8** and Movie S8 (Supporting Information). The droplet will spontaneously move from dark to light areas following the stripe, which acts as an optical

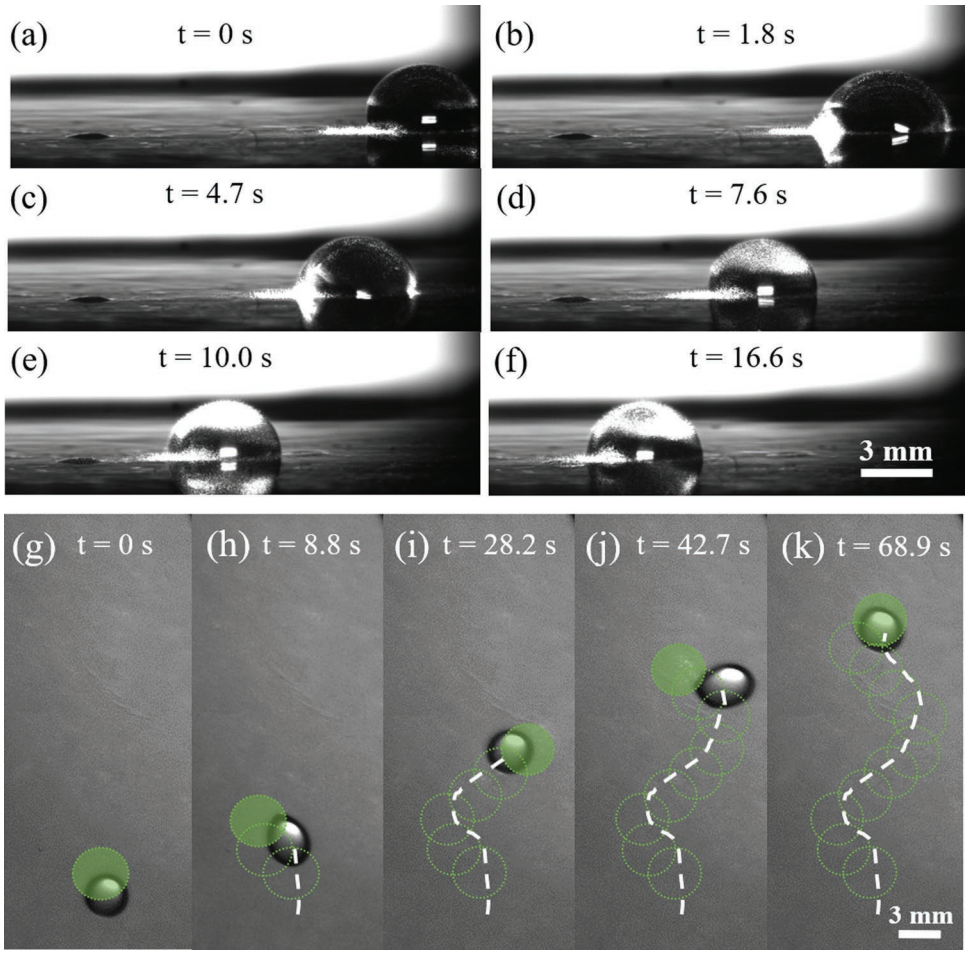

Figure 7. a–f) Sequential video frames showing the motion of a drop following a circular light spot uniformly illuminated shifted from right to left along a line (taken from the side) and g–k) along a wavy path (taken from the bottom). Empty circles indicate the positions occupied by the light spot throughout the video frames, and dashed lines represent the trajectory followed by the droplet. The experimental parameters are $I \approx 10.9$ kW m^{-2}, $D = 3$ mm, and $\Omega = 3$ µL.

conveyor belt. The main advantage of this design is that it does not require any moving parts: even the projected light pattern is static. It is somewhat the optical analog of the motion induced by a chemical gradient.[34]

Taking advantage of the SLM capabilities and considering the reproducibility of the response time, **Figure 9** shows that it is possible to move more droplets at a time until they merge, simultaneously illuminating different areas of the Fe:$LiNbO_3$/LIS surface. Two examples of the merging process are presented: in frames (a)–(d) (see also Movie S9 of the Supporting Information), the merging between two droplets moving in opposite directions is achieved with the simultaneous illumination of two circular spots gradually approaching each other. Instead, frames (e)–(h) (see also Movie S10 of the Supporting Information) show the merging of three drops moving along three different directions following the simultaneous illumination of three circular spots at different points on the sample.

Finally, we have investigated various strategies to induce the splitting of a water droplet into two subdroplets. In the literature, the splitting of microdroplets ($\Omega < 0.1$ µL) is reported only illuminating *y*-cut Fe:$LiNbO_3$ crystals,[20,35] where the photovoltaic field is oriented mainly along the crystal surface. Our preliminary results show that it is also possible to split a droplet by illuminating with a single spot a *z*-cut Fe:$LiNbO_3$ crystal. In this case, to induce the droplet elongation that eventually leads to the breakup, the light spot must be close to but off center the droplet, so that the electric field also assumes a nonmarginal in-plane component. For example, **Figure 10** reports a representative sequence of video frames showing the splitting of a 3 µL water drop induced by illuminating our *z*-cut crystals with a static, circular, and uniform light spot with $D = 3$ mm and $I \approx 19$ kW m^{-2}. In detail, frames (a)–(f) show the splitting as viewed from the bottom, while frames (A)–(F) show the simultaneous lateral view of the splitting of the same droplet. The bottom view (see also Movie S11 of the Supporting Information) suggests a quite complex scenario. Initially, the droplet is attracted toward the nearby illuminated spot, see frames (a), (b). Then, after about 7 s, it starts to slightly rotate and deform, see frames (c), (d). The elongation process continues, see frame (e), until the droplet breaks into two parts: the smaller one remains pinned to the light spot, while the larger one is pushed away. This process is obtained using an

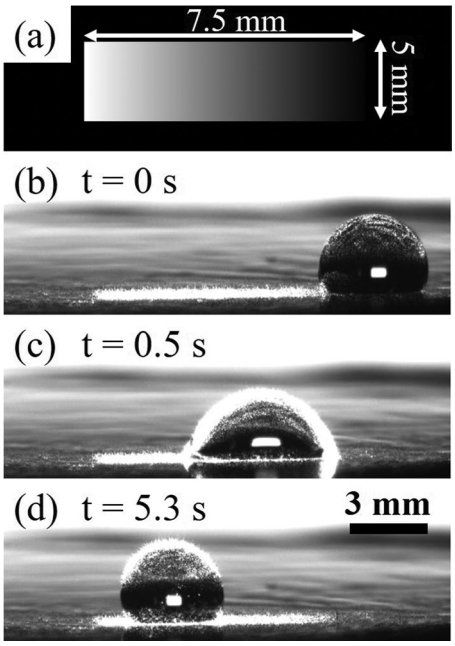

Figure 8. a) Image of the rectangular stripe presenting an increasing contrast used to generate the light pattern with the SLM. b–d) Sequential video frames taken from the side showing the motion of a 3 µL droplet along a rectangular stripe illuminated with an intensity that linearly increases from right, I_{min} = 0 kW m^{-2}, to left, I_{max} ≈ 7.2 kW m^{-2}.

intensity $I \approx 19$ kW m^{-2}, which is comparable to that used to split microdroplets sandwiched between two y-cut Fe:$LiNbO_3$ crystals,[35] but much lower than the value used to split hanging droplets from a 1 mm thick oil film.[37] More importantly, it was found that, to induce droplet splitting, the so-called light exposure rate,[20] equal to the product of light intensity by exposure time and thus proportional to the charge accumulated at the crystal surface, had to be greater than 200 kW s m^{-2}, that is more than 10 times the typical rates used to achieve droplet attraction. However, the observed phenomenology is quite complex because of the interplay between the capillary force induced by the water surface tension and the dielectrophoretic forces originated by the in-plane components of the photo-induced electric field. A detailed characterization of this rich process is beyond the scope of this work and will be the subject of a dedicated study.

4. Conclusions and Prospects

We have presented an optofluidic platform that performs the basic droplet handling operations required in a common open surface microfluidic device: guiding in both passive and active ways, merging, and splitting. It relies on z-cut, iron-doped lithium niobate crystals that, when illuminated, generate surface charges of opposite sign at the two crystal faces because of the photovoltaic effect. For robust and reliable manipulation of droplets, it is essential to coat the crystals with a lubricant-infused layer, which guarantees hydrophobicity and, more importantly, a very slippery surface whose properties are preserved even after prolonged use. In this way, sessile water droplets having volumes of microliters, which are more than three orders of magnitude higher than those reported in a previous study,[19] can be easily actuated, guided, merged, and split by the illumination of suitable static or dynamic optical patterns projected on the crystal, using a light intensity at least one order of magnitude lower than that previously reported.[19,30b] The actuated droplets can cover distances of centimeters within a timescale of a few seconds. These figures are similar to those typically achieved in electrowetting on dielectric devices that are already largely employed for various biological reactions, despite their cumbersome electrode connections.[36] This overall behavior is maintained for the handling of hundreds of droplets; in the event of deterioration of the lubricated coating, it can be easily refurbished with a simple dip-coating process.

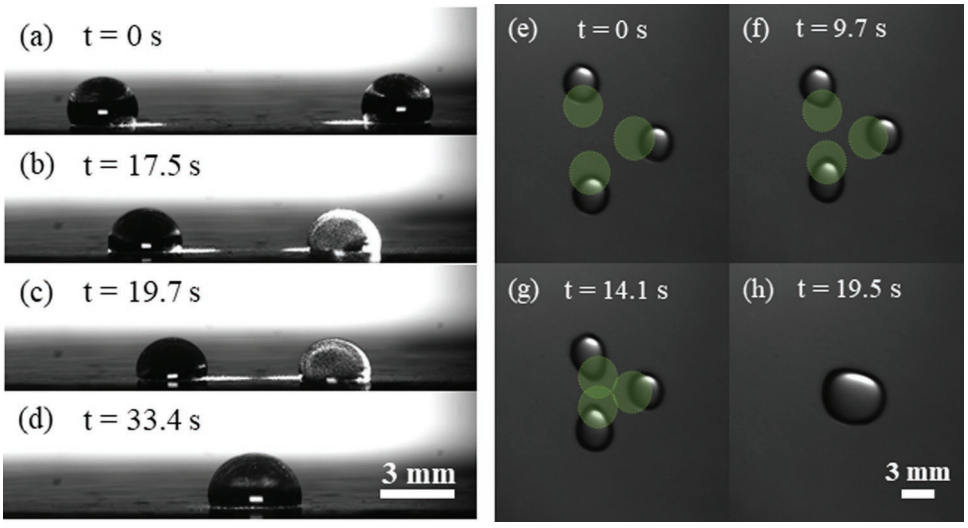

Figure 9. Sequential video frames showing the motion a–d) of two droplets as viewed from the side and e–h) of three droplets as viewed from the bottom following circular light spots. Light spots are generated at the same time on the Fe:$LiNbO_3$/LIS sample. The simultaneous actuation of the droplets leads to their merging. The experimental parameters are $I \approx 10.9$ kW m^{-2} for each spot, D = 3 mm, and Ω = 3 µL.

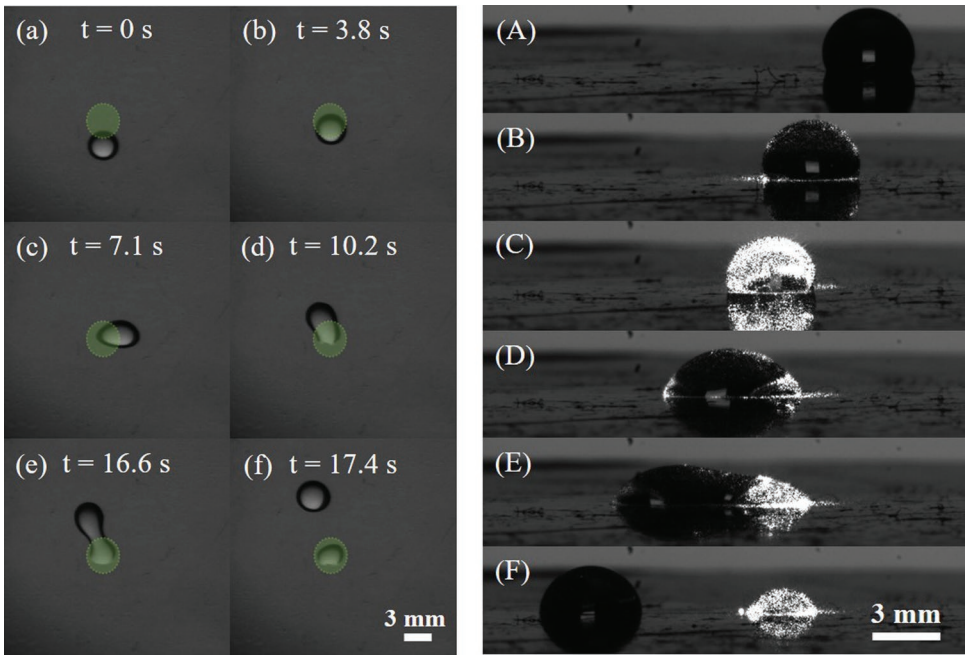

Figure 10. a–f) Sequential video frames showing the splitting of the same droplet as viewed from the bottom, and A–F) the corresponding simultaneous frames as viewed from the side. The laser spot is kept fixed in the same position throughout all frames. The experimental parameters are $D = 3$ mm, $\Omega = 3$ µL, and $P = 135$ mW, which corresponds to $I \approx 19.1$ kW m^{-2}.

Compared to existing methods used in open surface microfluidics,[1,37] the procedure is highly flexible and reconfigurable and does not require moving parts. Notably, the photoinduced virtual electrodes can be easily reprogrammed on the same Fe:$LiNbO_3$/LIS sample by waiting for spontaneous recombination of the charges within the crystal (typically, for some hours) or by immersing the whole sample for a few minutes in water, which ensures complete discharge without compromising the lubricant coating. Furthermore, the experimental setup can be naturally integrated with computer generated holograms displayed on SLM[38] and the adoption of new machine learning methods for the analysis of imaging data[39] that have been successfully applied to the manipulation of microparticles,[40] to make real-time decisions, such as controlling the motion of multiple droplets on Fe:$LiNbO_3$/LIS. As a result of all these useful features, it can be foreseen that this platform can find several applications in open surface microfluidics.[22]

Supporting Information

Supporting Information is available from the Wiley Online Library or from the author.

Acknowledgements

A.Z. and D.F. contributed equally to this work. The authors are particularly grateful to Giorgio Delfitto for his valuable technical assistance and to Sofia Saoncella, Luca Soravia, Andrea De Bei, and Giorgia Musso for their assistance in the acquisition of preliminary data. Partial funding from PRIN2017 UTFROM of the Italian Ministry of University and Research, from STARS Grant No. EXODROP, from BIRD Grant No. 165523/16 "Biosensing light-driven tools in advanced optomicrofluidic lithium niobate platform," and BIRD 2021 "BiodivSeq" of Padua University is kindly acknowledged.

Open access funding provided by Universita degli Studi di Padova within the CRUI-CARE Agreement.

Conflict of Interest

The authors declare no conflict of interest.

Data Availability Statement

The data that support the findings of this study are available from the corresponding author upon reasonable request.

Keywords

dielectrophoretic force, lithium niobate, lubricant infused surfaces, optofluidics, photovoltaic effect, wetting

Received: February 14, 2022
Revised: April 28, 2022
Published online: July 1, 2022

[1] a) J. S. Li, E. Ueda, D. Paulssen, P. A. Levkin, *Adv. Funct. Mater.* **2019**, *29*, 1802317; b) D. P. Regan, C. Howell, *Curr. Opin. Colloid Interface Sci.* **2019**, *39*, 137; c) X. D. Lou, Y. Huang, X. Yang, H. Zhu, L. P. Heng, F. Xia, *Adv. Funct. Mater.* **2020**, *30*, 1901130.
[2] Y. K. Lai, F. Pan, C. Xu, H. Fuchs, L. F. Chi, *Adv. Mater.* **2013**, *25*, 1682.

[3] D. Bonn, J. Eggers, J. Indekeu, J. Meunier, E. Rolley, *Rev. Mod. Phys.* **2009**, *81*, 739.
[4] C. Semprebon, S. Varagnolo, D. Filippi, L. Perlini, M. Pierno, M. Brinkmann, G. Mistura, *Soft Matter* **2016**, *12*, 8268.
[5] S. Varagnolo, D. Ferraro, P. Fantinel, M. Pierno, G. Mistura, G. Amati, L. Biferale, M. Sbragaglia, *Phys. Rev. Lett.* **2013**, *111*, 066101.
[6] S. Varagnolo, V. Schiocchet, D. Ferraro, M. Pierno, G. Mistura, M. Sbragaglia, A. Gupta, G. Amati, *Langmuir* **2014**, *30*, 2401.
[7] a) A. Lafuma, D. Quere, *EPL* **2011**, *96*, 56001; b) T.-S. Wong, S. H. Kang, S. K. Y. Tang, E. J. Smythe, B. D. Hatton, A. Grinthal, J. Aizenberg, *Nature* **2011**, *477*, 443.
[8] P. Sartori, D. Ferraro, M. Dassie, A. Meggiolaro, D. Filippi, A. Zaltron, M. Pierno, G. Mistura, *Commun. Phys.* **2022**, *5*, 81.
[9] S. K. Cho, H. J. Moon, C. J. Kim, *J. Microelectromech. Syst.* **2003**, *12*, 70.
[10] K. S. Khalil, S. R. Mahmoudi, N. Abu-dheir, K. K. Varanasi, *Appl. Phys. Lett.* **2014**, *105*, 041604.
[11] a) K. Ichimura, S. K. Oh, M. Nakagawa, *Science* **2000**, *288*, 1624; b) J. A. Lv, Y. Y. Liu, J. Wei, E. Q. Chen, L. Qin, Y. L. Yu, *Nature* **2016**, *537*, 179.
[12] F. Xia, L. Feng, S. T. Wang, T. L. Sun, W. L. Song, W. H. Jiang, L. Jiang, *Adv. Mater.* **2006**, *18*, 432.
[13] a) L. Y. Yeo, J. R. Friend, *Annu. Rev. Fluid Mech.* **2014**, *46*, 379; b) A. Wixforth, C. Strobl, C. Gauer, A. Toegl, J. Scriba, Z. von Guttenberg, *Anal. Bioanal. Chem.* **2004**, *379*, 982.
[14] a) F. Mugele, J. C. Baret, *J. Phys.: Condens. Matter* **2005**, *17*, R705; b) C. L. Hao, Y. H. Liu, X. M. Chen, Y. C. He, Q. S. Li, K. Y. Li, Z. K. Wang, *Sci. Rep.* **2014**, *4*, 6846.
[15] a) P. Y. Chiou, H. Moon, H. Toshiyoshi, C. J. Kim, M. C. Wu, *Sens. Actuators, A* **2003**, *104*, 222; b) S. Y. Park, M. A. Teitell, E. P. Y. Chiou, *Lab Chip* **2010**, *10*, 1655.
[16] a) K. Buse, *Appl. Phys. B: Lasers Opt.* **1997**, *64*, 273; b) K. Buse, *Appl. Phys. B: Lasers Opt.* **1997**, *64*, 391; c) A. Puerto, S. Coppola, L. Miccio, V. Vespini, A. Garcia-Cabanes, M. Carrascosa, P. Ferraro, *Adv. Mater. Interfaces* **2021**, *8*, 2101164.
[17] A. M. Glass, D. von der Linde, T. J. Negran, *Appl. Phys. Lett.* **1974**, *25*, 233.
[18] a) S. S. Sarkisov, M. J. Curley, N. V. Kukhtarev, A. Fields, G. Adamovsky, C. C. Smith, L. E. Moore, *Appl. Phys. Lett.* **2001**, *79*, 901; b) H. A. Eggert, F. Y. Kuhnert, K. Buse, J. R. Adleman, D. Psaltis, *Appl. Phys. Lett.* **2007**, *90*, 241909; c) X. Z. Zhang, J. Q. Wang, B. Q. Tang, X. H. Tan, R. A. Rupp, L. T. Pan, Y. F. Kong, Q. Sun, J. J. Xu, *Opt. Express* **2009**, *17*, 9981; d) M. Esseling, F. Holtmann, M. Woerdemann, C. Denz, *Opt. Express* **2010**, *18*, 17404; e) M. Carrascosa, A. Garcia-Cabanes, M. Jubera, J. B. Ramiro, F. Agullo-Lopez, *Appl. Phys. Rev.* **2015**, *2*, 040605; f) M. Esseling, A. Zaltron, W. Horn, C. Denz, *Laser Photonics Rev.* **2015**, *9*, 98; g) L. P. Chen, S. B. Li, B. L. Fan, W. B. Yan, D. H. Wang, L. H. Shi, H. J. Chen, D. C. Ban, S. H. Sun, *Sci. Rep.* **2016**, *6*, 29166; h) M. Gazzetto, G. Nava, A. Zaltron, I. Cristiani, C. Sada, P. Minzioni, *Crystals* **2016**, *6*, 123; i) J. F. Munoz-Martinez, A. Alcazar, M. Carrascosa, *Opt. Express* **2020**, *28*, 18085.
[19] B. L. Fan, F. F. Li, L. P. Chen, L. H. Shi, W. B. Yan, Y. Q. Zhang, S. B. Li, X. L. Wang, X. Wang, H. J. Chen, *Phys. Rev. Appl.* **2017**, *7*, 064010.
[20] A. Puerto, A. Mendez, L. Arizmendi, A. Garcia-Cabanes, M. Carrascosa, *Phys. Rev. Appl.* **2020**, *14*, 024046.
[21] X. Tang, W. Li, L. Q. Wang, *Nat. Nanotechnol.* **2021**, *16*, 1106.
[22] a) M. Hermann, P. Agrawal, I. Koch, R. Oleschuk, *Lab Chip* **2019**, *19*, 654; b) Y. Xu, A. M. Rather, Y. X. Yao, J. C. Fang, R. S. Mamtani, R. K. A. Bennett, R. G. Atta, S. Adera, U. Tkalec, X. G. Wang, *Sci. Adv.* **2021**, *7*, eabi7607.
[23] a) K. Peithmann, A. Wiebrock, K. Buse, *Appl. Phys. B: Lasers Opt.* **1999**, *68*, 777; b) L. Lucchetti, K. Kushnir, V. Reshetnyak, F. Ciciulla, A. Zaltron, C. Sada, F. Simoni, *Opt. Mater.* **2017**, *73*, 64.
[24] a) M. V. Ciampolillo, A. Zaltron, M. Bazzan, N. Argiolas, C. Sada, *Appl. Spectrosc.* **2011**, *65*, 216; b) S. Mignoni, M. D. Fontana, M. Bazzan, M. V. Ciampolillo, A. M. Zaltron, N. Argiolas, C. Sada, *Appl. Phys. B: Lasers Opt.* **2010**, *101*, 541.
[25] P. Sartori, E. Guglielmin, D. Ferraro, D. Filippi, A. Zaltron, M. Pierno, G. Mistura, *J. Fluid Mech.* **2019**, *876*, R4.
[26] C. J. Brinker, in *Chemical Solution Deposition of Functional Oxide Thin Films* (Eds: T. Schneller, R. Waser, M. Kosec, D. Payne), Springer, Vienna **2013**.
[27] A. Meggiolaro, S. Cremaschini, D. Ferraro, A. Zaltron, M. Carneri, M. Pierno, C. Sada, G. Mistura, *Micromachines* **2022**, *13*, 316.
[28] J. Villarroel, H. Burgos, A. Garcia-Cabanes, M. Carrascosa, A. Blazquez-Castro, F. Agullo-Lopez, *Opt. Express* **2011**, *19*, 24320.
[29] I. Nee, M. Muller, K. Buse, E. Kratzig, *J. Appl. Phys.* **2000**, *88*, 4282.
[30] a) X. Zhang, K. F. Gao, Z. X. Gao, Z. T. Zan, L. H. Shi, X. H. Liu, M. T. Wang, H. J. Chen, W. B. Yan, *Opt. Lett.* **2020**, *45*, 1180; b) X. Zhang, E. R. Mugisha, Y. H. Mi, X. H. Liu, M. T. Wang, Z. X. Gao, K. F. Gao, L. H. Shi, H. J. Chen, W. B. Yan, *ACS Photonics* **2021**, *8*, 639.
[31] D. Paulssen, S. Hardt, P. A. Levkin, *ACS Appl. Mater. Interfaces* **2019**, *11*, 16130.
[32] J. F. Munoz-Martinez, I. Elvira, M. Jubera, A. Garcia-Cabanes, J. B. Ramiro, C. Arregui, M. Carrascosa, *Opt. Mater. Express* **2015**, *5*, 1137.
[33] a) T. Podgorski, J. M. Flesselles, L. Limat, *Phys. Rev. Lett.* **2001**, *87*, 036102; b) M. Sbragaglia, L. Biferale, G. Amati, S. Varagnolo, D. Ferraro, G. Mistura, M. Pierno, *Phys. Rev. E* **2014**, *89*, 012406.
[34] S. Daniel, M. K. Chaudhury, J. C. Chen, *Science* **2001**, *291*, 633.
[35] F. F. Li, X. Zhang, K. F. Gao, L. H. Shi, Z. T. Zan, Z. X. Gao, C. Liang, E. R. Mugisha, H. J. Chen, W. B. Yan, *Opt. Express* **2019**, *27*, 25767.
[36] J. Li, C. J. Kim, *Lab Chip* **2020**, *20*, 1705.
[37] a) G. Mistura, M. Pierno, *Adv. Phys.: X* **2017**, *2*, 591; b) R. Malinowski, I. P. Parkin, G. Volpe, *Chem. Soc. Rev.* **2020**, *49*, 7879.
[38] R. Di Leonardo, F. Ianni, G. Ruocco, *Opt. Express* **2007**, *15*, 1913.
[39] B. Midtvedt, S. Helgadottir, A. Argun, J. Pineda, D. Midtvedt, G. Volpe, *Appl. Phys. Rev.* **2021**, *8*, 011310.
[40] a) E. Locatelli, M. Pierno, F. Baldovin, E. Orlandini, Y. Z. Tan, S. Pagliara, *Phys. Rev. Lett.* **2016**, *117*, 038001; b) G. Frangipane, D. Dell'Arciprete, S. Petracchini, C. Maggi, F. Saglimbeni, S. Bianchi, G. Vizsnyiczai, M. L. Bernardini, R. Di Leonardo, *eLife* **2018**, *7*, e36608.